Journal of Materials Chemistry C

Accepted Manuscript

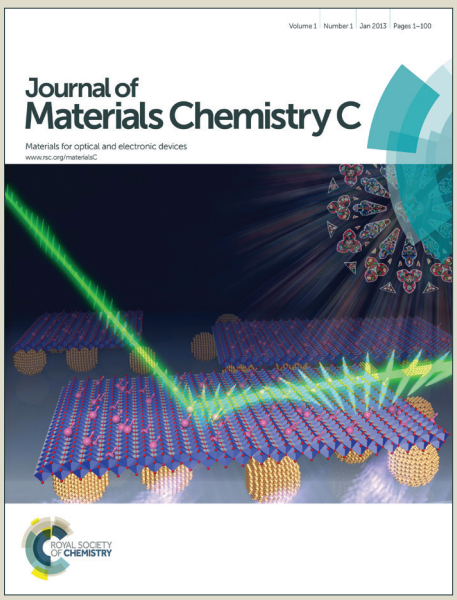

ROYAL SOCIETY OF CHEMISTRY

www.rsc.org/materialsC

Cite this: DOI: 10.1039/c0xx00000x

www.rsc.org/xxxxxx

ARTICLE TYPE

Tuning Memory Performances from WORM to Flash or DRAM by Structural Tailoring with Different Donor Moieties

Feng Zhou,[a] Jing-Hui He,[b] Quan Liu,[a] Pei-Yang Gu,[a] Hua Li,[a] Guo-Qin Xu,[b] Qing-Feng Xu*[a] and Jian-Mei Lu*[a]

Received (in XXX, XXX) Xth XXXXXXXXX 20XX, Accepted Xth XXXXXXXXX 20XX
DOI: 10.1039/b000000x

Four donor-acceptor organic molecules (HATT, HDTT, HETT and HRTT) consisting of different electron donors (phenol, triphenylamine, benzene and carbazole) and the same electron acceptor (triazole) were used as the active layer in NVM (nonvolatile memory) devices. I-V measurement showed that the ITO/HATT/Al and ITO/HETT/Al devices presented write-once-read-many-times (WORM) characteristics while TO/HDTT/Al exhibited a stable flash-type effect and the ITO/HRTT/Al device showed a volatile dynamic random access memory (DRAM) switching behaviour. These performances were well preserved when the electrodes changed to Pt. In order to elucidate the mechanisms associated with tunable memory behaviours, the effects of films/electrode interfaces, molecular simulation results were systematically investigated. We assigned the memory effects to the differences of the donor moieties. This study demonstrated that the electrical behaviours of organic materials could be switched by simply replacing the electron-rich groups with different charge delocalization abilities induced by the effect of electron donating ability and conjugation under an applied voltage, which would provide a guideline for the design of new materials with multitype high-performance memories.

Introduction

The electrical bistable materials have been extensively studied due to their potential application in the new generation of data storage devices such as NVM devices (Nonvolatile Memory) [1-12]. Small molecule-based memory devices[13-16] are becoming one of the most popular electrical memory materials due to their advantages of electrical bistability, well-defined molecular structures, versatility in molecular designs and good stimuli-responsive properties. It was well known that changes of electron-rich (donor) and electron-deficient (acceptor) moieties can effectively tune the molecular band gaps and frontier energy levels for organic electronic materials[17]. However, the relationship between the structures and memory performances of organic molecules was obscure and needed to be seriously studied. Up to now, the most commonly used method to obtain different memory types were the structural arrangements of donor–acceptor molecules[18, 19], the introduction of a π-spacer[20] and the optimization of electron-withdrawing groups[21]. Chen et al. revealed that the arrangements of donor (D)-accepter (A) moieties affected the electrical switching characteristics significantly[19]. However, the study on tuning memory performances through the alternative donor groups was less concerned. The triazole group is a strongly electron-deficient heterocycle with rich nitrogen atoms [22], which was often used to construct organic optoelectronic functional materials[23, 24]. In this paper, we selected four triazole-based organic molecules (HATT, HDTT, HETT and HRTT), in which phenol, triphenylamine, benzene or carbazole groups act as distinct donors (Scheme 1). The same acceptor and the different donors were linked by hydrazone bonds due to electroactive hydrazones with good charge-transporting properties and the simple synthesis[25]. Compared to the phenol and benzene groups, triphenylamine was a well-known candidate for holes transport materials in organic electronics due to its stable radical cations, good hole-mobility and limited charge delocalization[26]. Carbazole was used to study the influence of conjugation effect on switching behaviour. The introduction of phenol or benzene groups brought WORM behaviour, while triphenylamine and carbazole groups brought a stable flash-type and a DRAM effect, respectively. We found that donor groups with different electron donating ability and conjugation effect would change the electron density distributions and charge delocalization abilities of organic molecules themselves, which could tune the memory behaviors of devices effectively. The experimental results suggested that independent fine-tuning memory characteristics would be achieved by the changes of donor units.

Experimental

Materials

4-amino-3-hydrazino-5-mercapto-1, 2, 4-triazole (99%) was purchased from Alfa Aesar. Benzaldehyde, carbazole, p-Fluorobenzaldehyde, 4-(N, N-Diphenylamino) benzaldehyde, salicylaldehyde and formic acid were purchased from Shanghai

Sinopharm Co. Ltd. All reagents were used as received from commercial sources without any further purification.

Apparatus

^{1}H and ^{13}C NMR spectra were measured on an INOVA 400MHz spectrometer with d6-dimethyl sulfoxide (DMSO) as the solvents. Elemental analysis of C, H and N were conducted on a Carlo Erba-MOD1106 elemental analyzer. UV-Visible absorption Spectra was recorded on a Perkin-Elmer λ-17 spectrometer. Thermogravimetric analysis (TGA) was conducted on a TA instrument Dynamic TGA 2950 at a heating rate of 10 °C•min^{-1} under a N_2 flow rate of 50 mL•min^{-1}. Cyclic voltammetry (CV) measurement was performed on a CHI-660C electrochemical workstation using an indium-tin oxide (ITO) plate as the working electrode, a platinum wire as the auxiliary electrode, and an Ag/AgCl (KCl saturated) electrode as the reference electrode. A 0.1 M solution of tetra-butylammonium hexafluorophosphate (n-Bu_4NPF_6) in anhydrous acetonitrile was employed as the supporting electrolyte. SEM images were taken on a Hitachi S-4700 scanning electron microscope. The films were formed using the J5Z32H400 high vacuum thermal evaporation equipment. Atomic force microscopy (AFM) measurements were performed using a MFP-3DTM (Digital Instruments/Asylum Research) AFM instrument. The devices were characterized at room temperature under ambient conditions, using a Hewlett-Packard 4145B semiconductor parameter analyzer with Hewlett-Packard 8110A pulse generator. The fluorescence spectra were measured on Edinburgh-920 fluorescence spectra photometer (Edinburgh Co.UK) with a slit of 3 nm.

Synthesis of compounds

Synthesis of HATT The synthesis and characterization of HATT were reported in our previous work[27].

Synthesis of HDTT HDTT was synthesized by a similar procedure as HATT. The crude product was purified by recrystallization from acetone in 65% yield. ^{1}H NMR (400 MHz, DMSO-d_6) δ= 12.90 (s, 1H), 10.52 (s, 1H), 8.23 (s, 1H), 7.49 (d, J=8.5 Hz, 2H), 7.34 (t, J= 7.7 Hz, 4H), 7.08 (dd, J= 19.2, 7.6 Hz, 6H), 6.94 (d, J= 8.4 Hz, 2H), 5.49 ppm (s, 2H). ^{13}C NMR (75 MH_Z, [D6] DMSO): δ = 163.94, 149.31, 147.78, 146.33, 143.37, 129.32, 127.93, 127.22, 124.27, 123.34, 121.59 ppm; Elemental analysis calcd (%) for $C_{21}H_{19}N_7S$: C 62.82, H 4.77, N 24.42. Found: C 62.76, H 4.64, N 24.54.

Synthesis of HETT and HRTT The synthesis and characterization of HETT and HRTT were listed in supporting information.

Fabrication of memory devices

Fabrication and measurements of the ITO/HATT/Al, ITO/HDTT/Al, ITO/HETT/Al and ITO/HRTT/Al electrical memory devices The indium-tin oxide (ITO) glass was precleaned by sonicating for 15 min with deionized water, acetone and ethanol, sequentially. Then the HATT, HDTT, HETT and HRTT were deposited onto the surface of the ITO under a pressure of 10^{-6} Torr. The thickness of the film was typically about 70 nm, which were traced by a calibrated quartz crystal monitor. Finally, Al was thermally evaporated and deposited onto the film surface at about 10^{-7} Torr through a shadow mask to yield top electrodes with thickness around 100 nm and area of 0.0314 mm^2. The fabricated memory device was shown in Scheme 1b. The devices were characterized at room temperature under ambient conditions, using a Hewlett-Packard 4145B semiconductor parameter analyzer.

Fabrication and measurements of the Si/Pt/HATT/Pt and Si/Pt/HDTT/Pt electrical memory devices The Si/Pt substrate was precleaned by sonication for 15 min with deionized water, acetone and ethanol. Then HATT and HDTT were deposited onto the surface of the Si/Pt substrate under a pressure of 10^{-6} Torr. Pt was sputtered onto to the film surface through a shadow mask yield top electrodes.

Computational details

All calculations were based on density functional theory (DFT) with generalized gradient approximation (GGA), which is implemented in DMol^3 code.[28] Unrestricted BLYP/DNP level of theory was used to optimize the geometries and calculate the total energies of molecules in charged states of -2, -1, 0, +1 and +2 with convergence criteria in energy and force of 2×10^{-4} eV and 0.02 eV/Å, respectively. The isosurfaces of total electron density at 10^{-4}/Å^3 was plotted to render the molecular electrostatic potentials (ESP), and an isovalue of 0.015/Å^3 was used for drawing the orbitals. The lowest excitation energies of molecules were roughly estimated by HOMO-LUMO gap in the ground states.

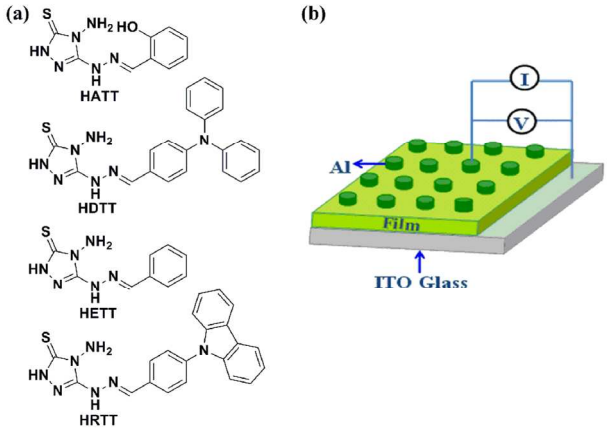

Scheme 1 (a) The chemical structure of compounds HATT, HDTT, HETT and HRTT; (b) Scheme of the sandwich devices.

Results and discussion

Thermal stabilities

The thermal stabilities of four small molecules were evaluated by TGA under a nitrogen atmosphere at a heating rate of 10 ^{o}C min^{-1}. As shown in the TGA curves (Figure S10), the thermal decomposition temperatures (the 5% weight-lost temperature) of HATT, HDTT, HETT and HRTT were up to 266, 264, 258 and 271 ^{o}C, respectively. The good-thermal stability of the four active materials would endure heat deterioration in the memory devices.

Optical properties

Figure 1 showed the optical absorption spectra of HATT, HDTT, HETT and HRTT in DMF solution and thin solid film states. The absorption spectrum of HATT solution was featured with two absorption bands (Figure 1a). The maximum absorption at 270 nm and 332 nm were attributed to a π-π* transition of aromatic rings and a typical intramolecular charge transfer between the phenol (the donor) and triazole part group (the accepter) respectively. As shown in Figure 1b, the absorption spectra of HDTT solution showed two peaks at 300 nm and 364 nm, ascribed to an aromatic π-π* transition and an intramolecular charge transfer from the triphenyl amine to triazole units, respectively. HETT (λ_{abs}= 264, 316 nm) and HRTT (λ_{abs}= 291, 342 nm) solution also exhibited two absorption bands, as shown in Figure 1c and Figure 1d. Compared with the absorption spectra in solution, the thin films of compound HATT and HETT exhibited strongly broadened absorption peaks and that of HDTT showed slightly bathochromic–shift and broadened absorption bands. However, the absorption bands of HRTT in the solid state showed a hypsochromic-shift absorption relative to that in solution, indicating the formation of H-aggregates. The formation of H-aggregate was likely due to the introduction of the conjugated carbazole group. The red/ blue-shifted and broadened absorption peaks from solutions to film states might be associated with molecular aggregation and/or increased polarity[18], which was beneficial for the improvement of the charge carrier mobility of the nanofilm under an applied electric field[29].

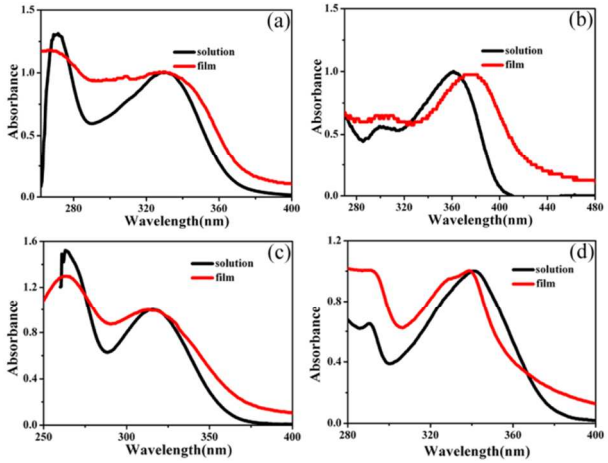

Fig. 1 Normalized UV-vis absorption spectra of DMF solution (black) and thin solid film on a quartz plate (red) of as-synthesized small molecules: (a) HATT, (b) HDTT, (c) HETT and HRTT (d).

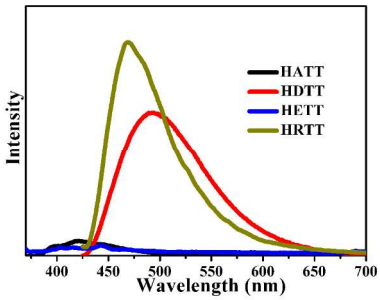

Fig. 2 PL spectra of HATT, HDTT, HETT and HRTT in $CHCl_3$ solvent. Excitation wavelength was fixed at 360 nm.

In order to further investigate the photoinduced intramolecular events, the photoluminescence (PL) spectrum of HATT, HDTT, HETT and HRTT were measured (Figure 2). The fluorescence spectra of HATT and HETT were considerably quenched as compared to those HDTT and HRTT, indicating that the different charge-separated states for HATT (HETT) and HDTT (HRTT). The permanent charge-separated state in the excited states of HATT and HETT between D–A parts resulted in the intramolecular quenching process[30, 31].

Electrochemical properties

Table 1 Optical and electrochemical properties of the four films.

Sample	Film (nm)		E_g[a]	E[b] (V)	HOMO[c]	LUMO
	λ_{max}	λ_{onset}	(eV)	E_{ox}(onset)	(eV)	(eV)
HATT	330	380	3.26	1.16	–5.48	–2.22
HDTT	376	446	2.78	0.97	-5.29	-2.51
HETT	315	375	3.31	1.25	-5.57	-2.26
HRTT	339	386	3.20	1.05	-5.37	-2.17

[a] The data were calculated by the following equation: bandgap = 1240/λ_{onset} of films. [b] Vs Ag/AgCl in anhydrous MeCN. [c] The energy levels of the HOMO were calculated from cyclic voltammetry and were referenced to ferrocene (0.48 eV).

Figure S12 showed the cyclic voltammograms (CVs) of the four films on ITO glass substrates in 0.1 M acetonitrile solution of tetrabutylammonium hexafluorophosphate. The highest occupied molecular orbital (HOMO) and lowest unoccupied molecular orbital (LUMO) energy levels of the four films could be calculated from the optical band gap (E_g) and the onset oxidation potential (Eox^{onset}) based on the reference energy level of ferrocene/ferricinium ion couple (E_{FOC}) by the following equations respectively: $E_{HOMO} = -[E_{ox}^{onset} + 4.8 - E_{Foc}]$, $E_{LUMO} = E_{HOMO} + E_g$. The optical band gaps (E_g) of HATT, HDTT, HETT and HRTT were estimated to 3.26, 2.78, 3.31, 3.20 eV, respectively. The HOMO energy levels of the four films were determined to be -5.48, -5.29, -5.57 and -5.37 eV, and the LUMO energy levels of the four films were determined to be -2.22, -2.51, -2.26 and -2.17 eV (Table 1). The energy barriers between the work functions (Φ) of ITO bottom electrodes (-4.8 eV) and the HOMO energy levels of HATT, HDTT, HETT and HRTT were 0.68, 0.49, 0.77 and 0.57 eV, which were much lower than the energy barriers of 2.06, 1.77, 2.02 and 2.11 eV between the work functions (Φ) of the Al top electrodes and LUMO energy levels of the four films (Figure 5b). The lower energy barriers were expected to be beneficial for enhancing the hole injection from ITO into the four electroactive thin films, which indicated that holes predominated the conduction process in the devices. Hence, the four molecules exhibited the p-type semiconductor characteristics[32].

Morphology of films

Atomic force microscopy (AFM) was used to characterize the surface morphologies and roughness of the vacuum-deposited electroactive layers. As shown in Figure 3, the AFM topography images clearly showed HATT formed well-developed network morphology and HETT was provided with a grain-like morphology, however HDTT and HRTT films possessed disordered aggregation. The surface root-mean-square (RMS) roughness of the HATT, HDTT, HETT and HRTT thin films

were 1.214, 6.77, 0.743, 0.907 nm, respectively. The small surface roughness in the AFM images of the films lead to the good quality of the films, which could offer a strong guarantee for high-performing data-storage devices. We preformed X-ray diffraction analysis to understand the crystallinity of the films. There were no bragg reflection peaks without the peak of the quartz substrate (Figure S13), which revealed the four films were all amorphous. According to the previous reports[33, 34], the self-assembly induced by hydroxyl groups and fine planarity could promote molecular aggregation, so the special morphologies of the HATT and HETT films was attributed to the self-assembly and planarity.

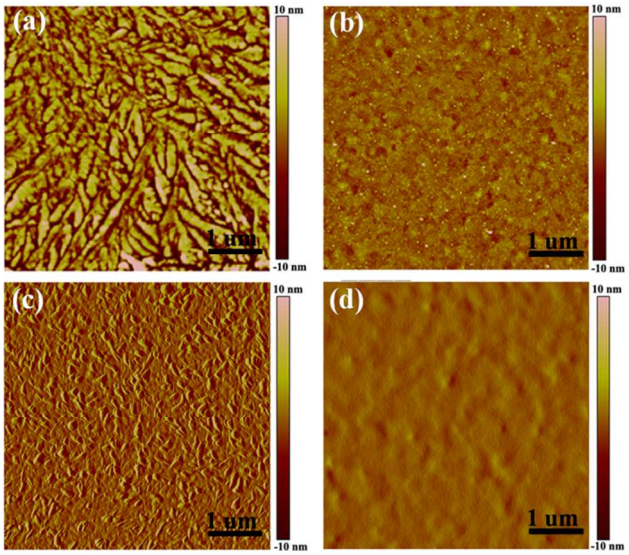

Fig. 3 Tapping-mode (5 um×5 um) AFM topographies of: (a) HATT, (b) HDTT, (c) HETT and HRTT films.

Memory Effects

For avoiding the effect of films thickness on the devices performance[35], the thicknesses of HATT, HDTT, HETT and HRTT films were controlled by a high vacuum thermal evaporation method. As shown in Figure S14, the thickness of HATT (69 nm), HDTT (73 nm), HETT (71nm) and HRTT (75 nm) films were with the similar scales.

The memory effects of HATT and HDTT based devices were demonstrated by the current-voltage characteristics as shown in Figure 4. In the first sweep from 0 to -6 V, the injection current of ITO/HATT/Al device increased progressively with the applied bias and a sharp increase from 10^{-6} A to 10^{-2} A was observed at the switching threshold voltage of -4.3 V, which indicated that the device switched from a low-conductivity state (OFF state) to a high-conductivity state (ON state). The OFF-to-ON was regarded as a "writing" process in a memory cell. The cell kept good stability in the ON state during the subsequent negative sweep from 0 to -6 V (sweep 2) even after applying a positive sweep from 0 to 6 V (sweep 3). The I-V characteristic revealed that HATT-based device exhibited the electrical bistability and a nonvolatile WORM-type memory effect. The stability of the HATT device under a constant stress of -1 V was shown in Figure 4c. No significant degradation existed in current for ON and OFF states for at least 200 min during the test, which promised a low misreading rate due to the precise control of the ON and OFF states. Then, the effect of continuous read pulses with a read voltage of -1 V on the ON and OFF states was investigated (Figure 4e). As shown in Figure 4e (inset), no resistance degradation was observed for ON and OFF states after more than 10^6 read cycles. Thus, both states were stable under voltage stress and were insensitive to read pulses.

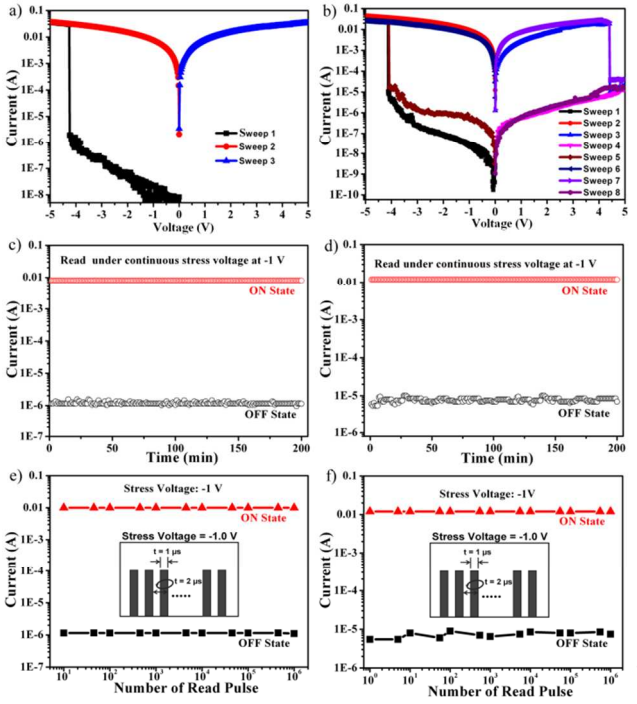

Fig. 4 Typical current-voltage (I-V) characteristics of the memory devices in the ON and OFF states fabricated with: (a) HATT and (b) HDTT; Retention times on the ON and OFF states of (c) ITO/HATT/Al and (d) ITO/HDTT/Al devices under a constant stress of -1.0 V; Effect of read pulses of -1 V on the ON and OFF states of (e) ITO/HATT/Al and (f) ITO/HDTT/Al devices.

Compared to the ITO/HATT/Al device, ITO/HDTT/Al presented a nonvolatile bistability flash-type memory effect as shown in Figure 4b. As the initial voltage swept from 0 to -6 V, the current density increased progressively with the applied bias and a sharp increase in the injection current at about -4.0 V (the first sweep), indicating the device transition from OFF state ("0" signal) to ON state ("1" signal) . The transition from OFF state to ON state was served as the "writing" process. For the subsequent negative sweep from 0 to -6 V, the storage cell maintained in the ON state (the second sweep). The I-V effects defined the electrical bistability of HDTT and also revealed the nonvolatile nature of the memory effect. In the fourth reverse sweep from 0 to 6.0 V, an abrupt decrease in current was observed at the threshold voltage of about 4.1 V, which was equivalent to the "erasing" process. The fifth to eighth sweeps revealed that the write-read (ON)-erase-read (off) switching cycles were repeatable with high accuracy. This memory features suggested that the memory device exhibited flash-type memory. The parameters of ON/OFF current ratios, read cycles and retention ability were investigated to study the performance of the memory device. The 10^3 ON/OFF current ratio promised a low misreading rate through the precise control of the ON and OFF states. There was no significant

degradation of the device in both the ON and OFF states after 200 min of the continuous stress test (Figure 4d). Moreover, no degradation in current density was observed for the ON and OFF states after more than 10^6 read cycles (Figure 4f).

In addition, the device based on HETT exhibited non-volatile write-once-read-many-times (WORM) characteristics (Figure 5a), and the ITO/HRTT/Al device was equipped with dynamic random access memory (DRAM) effects (Figure 5b).

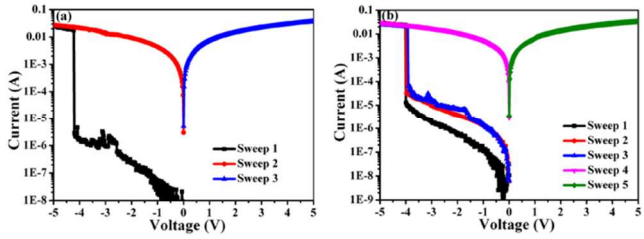

Fig. 5 Typical current-voltage (I-V) characteristics of the memory devices in the ON and OFF states fabricated with: (a) HETT and (b) HRTT.

Mechanisms of the memory devices

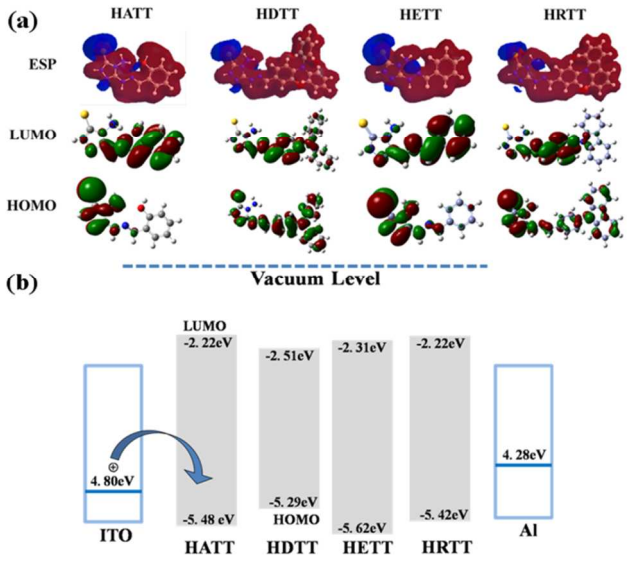

Fig. 6 (a) Simulated molecular orbitals, charge distributions and electrostatic potential plots of the four molecules in their optimized ground-state structures. The plotting parameters were described in the section of computational details; (b) Energy levels of the HOMO and LUMO of the four molecules along with the work function of the electrodes.

It has been reported that the electron located on the electron donor part which totally transits to the electron acceptor part under electric field would form a permanent charge-separated state and shows a WORM-type characteristic, yet the transition which the electron located on donor side partly or slightly transit to the acceptor side could be easily detrapped through reverse voltage or even automatically revert to the pristine state and thus lead to a flash or DRAM memory performance[36]. The density functional theory (DFT) simulation results showed that the electron density distribution of the HOMO orbital of HATT was mainly located on the triazole moiety whereas the LUMO orbital mainly distributed on the phenol group (Figure 6a). This distinct asymmetric distributions of the HOMO and LUMO indicated an obvious electron pull-push effect. When HATT was activated under an applied voltage, the electron density in excited state observably transferred from the donor to acceptor side. Charge carriers with low energy could not overcome the injection barrier between the donor (D) and acceptor (A) under a low voltage bias, therefore the devices kept in the OFF state. Based on the variation of orbital and system energies versus charges, the values of HOMO, LUMO and their band gaps reduced along with the addition of charges (Figure 7a and Table S1), which would cause the increased conductivity of molecules. When the external applied bias increases to the threshold voltage, carriers and current density would increase sharply. Hence, the devices could transit from OFF state to the ON state. The obvious electron pull-push effect would cause a permanent charge-separated state. Because of the permanent charge-separated state, the ON state could sustain after the removal of external field or even under an applied reverse bias. Hence, the ITO/HATT/Al device exhibited a nonvolatile WORM-type memory effect.

The calculated electron density distributions of the HOMO and LUMO for HDTT were summarized in Figure 6b. The new donor (triphenylamine) with limited charge delocalization played a significant role in electron density distributions. The electron density was not only located on the electron donor (triphenyl amine) side but also located on the electron acceptor side (triazole), indicating that the electron pull-push effect was not obvious. While the HDTT was activated by electrical stimulation, the electron density in excited state transferred from the triphenylamine moiety to triazole side slightly. Similar to HATT, the electron density transition from HOMO to LUMO lead the surge in carrier and current density and the corresponding transition from the OFF to the ON state[18]. The less obvious electron pull-push effect of HDTT would bring an unstable charge-separated state, which could be dissociated and the device would revert to the pristine state (OFF state) under an applied reverse bias[37]. Therefore, the ITO/HATT/Al device presented a nonvolatile flash-type memory behavior. Compared to the threshold voltage of ITO/HATT/Al device (-4.3 V), the ITO/HDTT/Al device possesses a lower switch-on voltage (-4.0 V), which was consistent with energy barriers (0.68, 0.49 eV) between the anode (ITO) and the HOMO energy levels of HATT and HDTT.

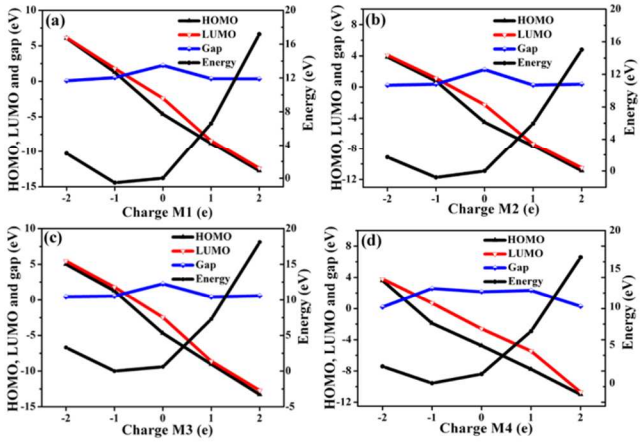

Fig. 7 Variation of orbital and system energies versus charges: (a) HATT, (b) HDTT, (c) HETT and (d) HRTT.

In order to further study the influence of films/electrodes

interface on the memory behaviors, we used metal Pt instead of Al top electrode to rule out the metal filament mechanism[38]. The measured I-V curves (Figure 8) showed that Si/Pt/HATT/Pt and Si/Pt/HDTT/Pt devices also exhibited a WORM-type memory effect and a flash-type memory behavior, respectively. Because of lower energy barriers (0.12, 0.31 eV) between the work functions (Φ) of Pt (5.6 eV) and the HOMO levels of HATT and HDTT than that with Al electrode ((0.68, 0.49 eV), the threshold voltage decreases significantly based on the Pt electrode. Therefore, we could draw a conclusion that the molecular structure effects should control the I–V performance rather than metal diffusion.

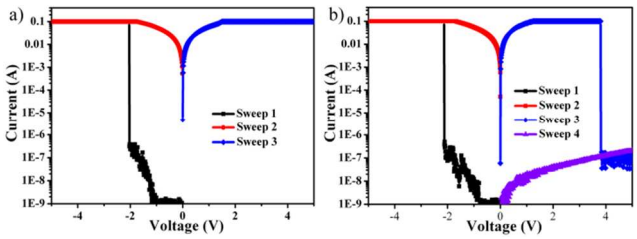

Fig. 8 Current-voltage (I-V) characteristics of Si/Pt/HATT/Pt device (a) and Si/Pt/HDTT/Pt device (b).

According to the theoretical calculation and related experiments, the electron donating ability played a key role in the charge delocalization of the donors and the memory behaviour. The calculated electron density distribution of the HOMO and LUMO for HETT was similar as that of HATT and the distinct asymmetric distributions of the HOMO and LUMO also indicated an obvious electron pull-push effect. However, the symmetric distributions of the HOMO, LUMO of HDTT and HRTT revealed an inconspicuous electron pull-push effect (Figure 6). The ITO/HETT/Al device also presented a WORM-type memory behavior, and it was as same as ITO/HATT/Al device. Then, the conjugation effect was found to be closely linked with the memory behaviour. Compared to ITO/HDTT/Al device, the ITO/HRTT/Al device showed a DRAM-type memory effect. HDTT and HRTT both exhibited inconspicuous electron pull-push effects, yet the conjugated carbazole could increase the electron mobility and the electron could be easily detrapped automatically.

Based on the theoretical calculations, photoluminescence (PL) spectra and comparative analysis of structures, the glaring discrepancy of electrical switching behaviors for the ITO/HATT/Al, ITO/HDTT/Al, ITO/HETT/Al and ITO/HRTT/Al devices may be attributed to the different variations of orbital/system energies and the following charge-separated states between the same acceptor and the different donor under electric field, which was due to the donors with different charge delocalization abilities[26, 39]. The divergences in charge delocalization abilities were closely related to the effect of electron donating ability and conjugation. The stable charge separation state of HATT and HETT hindered the electron density from back recombination even under the reverse bias. Yet, HDTT/HRTT-based devices underwent an unstable charge delocalization state and the state could revert to its original state through reverse voltage or automatically.

Conclusion

In summary, four new electroactive hydrazine derivatives (HATT, HDTT, HRTT and HETT) with different donor groups were employed as active layers for memory devices with different performances. HATT/ HETT-based device presented the WORM effect, while HDTT-based device exhibited the flash nature and HRTT-based device showed the DRAM effect. Mechanism analysis indicated that the differences in their behaviors was due to the different charge delocalization abilities of four donors with discrepant effects of electron donating ability and conjugation and the following differences in charge separation states. This result made a further step toward realizing tunable multitype memory device performances by structural tailoring with different donor groups.

Acknowledgements

The authors appreciate finance support from Chinese Natural Science Foundation (21371128 and 21336005), Chinese-Singapore Joint Project (2012DFG41900) and the Specialized Research Fund for the Doctoral Program of Higher Education of China (grant no.20113201130003).

Notes and references

[a]College of Chemistry, Chemical Engineering and Materials Science, Collaborative Innovation Center of Suzhou Nano Science and Technology, Soochow University, Suzhou, 215123, China. Fax: +86 512 65880367; Tel: +86 512 65880368; E-mail: lujm@suda.edu.cn, xuqingfeng@suda.edu.cn.

[b]Department of Chemistry, National University of Singapore, 117543, Singapore.

Electronic Supplementary Information (ESI) available: [^{1}H NMR (DMSO -d6) of HATT (Figure S1); ^{13}C NMR spectrum of HATT in DMSO-d6 (Figure S2); ^{1}H NMR (DMSO-d6) of HDTT (Figure S3); ^{13}C NMR spectrum of HDTT in DMSO-d6 (Figure S4); Cross-sectional SEM images of the ITO/HATT/Al (a) and ITO/HDTT/Al (b) devices (Figure S5)]. See DOI: 10.1039/b000000x/

1 J. C. Scott, L. D. Bozano, *Adv. Mater.*, 2007, **19**, 1452.
2 B. Koo, H. Baek, J. Cho, *Chem. Mater.*, 2012, **24**, 1091.
3 T. W. Kelley, P. F. Baude, C. Gerlach, D. E. Ender, D. Muyres, M. A. Haase, D. E. Vogel, S. D. Theiss, *Chem. Mater.*, 2004, **16**, 4413.
4 Y. Ko, Y. Kim, H. Baek, J. Cho, *ACS Nano.*, 2011, **5**, 9918.
5 Q. –D. Ling, D. –J. Liaw, C. X. Zhu, D. S. -H. Chan, E. -T. Kang, K. -G. Neoh, *Progress in Polymer Science.*, 2008, **33**, 917.
6 C. W. Chu, J. Y. Ouyang, J. -H. Tseng, Y. Yang, *Adv. Mater.*, 2005, **17**, 1440.
7 Q. Ling, Y. Song, S. J. Ding, C. Zhu, D. S. H. Chan, D. -L. Kwong, E. -T. Kang, K. -G. Neoh, *Adv. Mater.*, 2005, **17**, 455.
8 S. -J. Liu, Z. H. Lin, Q. Zhao, Y. Ma, H. -F. Shi, M. -D. Yi, Q. -D. Ling, Q. -L. Fan, C. -X. Zhu, E. -T. Kang, W. Huang, *Adv. Funct. Mater.*, 2011, **21**, 979.
9 P. Heremans, G. H. Gelinck, R. Müller, K. -J. Baeg, D. -Y. Kim, Y. -Y. Noh, *Chem. Mater.*, 2011, **23**, 341.
10 S. Choi, S. -H. Hong, S. H. Cho, S. Park, S. -M. Park, O. Kim, M. Ree, *Adv. Mater.*, 2008, **20**, 1766.
11 G. Sun, J. Liu, L. Zheng, W. Huang, H. Zhang, *Angew. Chem. Int. Ed.*, 2013, **52**, 13351.
12 J. Liu, Z. Yin., X. Cao., F. Zhao, L. Wang, W. Huang, H. Zhang, *Adv. Mater.*, 2013, **25**, 233.
13 H. Jiang, H. P. Zhao, K. K. Zhang, X. D. Chen, C. Kloc, W. P. Hu, *Adv. Mater.*, 2011, **23**, 5075.
14 H. Li, Q. F. Xu, N. J. Li, R. Sun, J. F. Ge, J. M. Lu, H. W. Gu, F. Yan, *J. Am. Chem. Soc.*, 2010, **132**, 5542.

15 Y. L. Shang, Y. Q. Wen, S. L. Li, S. X. Du, X. B. He, L. Cai, Y. F. Li, L. M. Yang, H. J. Gao, Y. L. Song, *J. Am. Chem. Soc.*, 2007, **129**, 11674.
16 Y. -C. Lai, T. Kurosawa, T. Higashihara, M. Ueda, W. -C. Chen, *Chem. Asian J.*, 2013, **8**, 1514.
17 P. J. Homnick, P. M. Lahti, *Phys. Chem. Chem. Phys.*, 2012, **14**, 11961.
18 Y. Ma, X. B. Cao, G. Li, Y. Q. Wen, Y. Yang, J. X. Wang, S. X. Du, L. M. Yang, H. J. Gao, Y. L. Song, *Adv. Funct. Mater.*, 2010, **20**, 803.
19 W. -Y. Lee, T. Kurosawa, S. -T. Lin, T. Higashihara, M. Ueda, W. -C. *Chen, Chem. Mater.*, **2011**, 23, 4487.
20 G. Wang, S. F. Miao, Q. J. Zhang, H. F. Liu, H. Li, N. J. Li, Q. F. Xu, J. M. Lu, *Chem. Commun.*, 2013, **49**, 9470.
21 S. F. Miao, Y. X. Zhu, H. Zhuang, X. P .Xu, H. Li, R. Sun, N. J. Li, S. J. Ji, J. M. Lu, *J. Mater. Chem. C.*, 2013, **1**, 2320.
22 M. Juricek, P. H. J. Kouwer, A. E. Rowan, *Chem. Commun.*, 2011, **47**, 8740.
23 Y. T. Tao, Q. Wang, L. Ao, C. Zhong, C. L. Yang, J. G. Qin, D. G. Ma, *J. Phys. Chem. C.*, 2010, **114**, 601.
24 Z. H. Li, M. S. Wong, H. F., Y. Tao, *Org. Lett.*, 2006, **8**, 4271.
25 R. Lygaitis, V. Getautis, J. V. Grazulevicius, *Chem. Soc. Rev.*, 2008, **37**, 770.
26 Z. F. Yang, B. Xu, J. T. He, L. L. Xue, Q. Guo, H. J. Xia, W. J. Tian, *Organic Electronics.*, 2009, **10**, 954.
27 F. Zhou, P. L. Tan, Y. Ma, Y. Y. Li, N. J. Li, H. Li, L. H. Wang, H. W. Gu, Q. F. Xu, J. M. Lu, *Chem. Asian J.*, 2014, **9**, 223.
28 B. Delley, *J. Chem. Phys.*, 2000, **113**, 7756.
29 R. Schmidt, J. H. Oh, Y. -S. Sun, M. Deppisch, A. -M. Kraüse, K. Radacki, H. Braunschweig, M. Könemann, P. Erk, Z. Bao, F. Wurthner, *J. Am. Chem. Soc.*, **2009**, 131, 6215.
30 G. J. Kavarnos, N. J. Turro, *Chem. Rev*., 1986, **86**, 401.
31 C. V. Suneesh, B. Balan, H. Ozawa, Y. Nakamura, T. Katayama, M. Muramatsu, Y. Nagasawa, H. Miyasaka, K. Sakai, *Phys. Chem. Chem. Phys.*, 2014, **16**, 1607.
32 Y. Li, R. Fang, S. Ding, Y.Shen, *Macromol. Chem. Phys.*, 2011, **212**, 2360.
33 D. Feyter, F. C. D. Schryver, *Chem. Soc. Rev.*, 2003, **32**, 139.
34 T. S. Balaban, *Acc. Chem. Res.*, 2005, **38**, 612.
35 S. Park, T. J. Lee, D. M. Kim, J. C. Kim, K. Kim, W. Kwon, Y. -G. Ko, H. Choi, T. Chang, M. Ree, *J. Phys. Chem. B.*, 2010, **114**, 10294.
36 T. Kuorosawa, C. -C. Chueh, C. -L. Liu, T. Higashihara, M. Ueda, W. -C. Chen, *Macromolecules.*, 2010, **43**, 1236.
37 N. -H. You, C. -C. Chueh, C. -L. Liu, M. Ueda, W. -C. Chen, *Macromolecules.*, 2009, **42**, 4456.
38 W. -J. Joo, T. -L. Choi, J. Lee, S. K. Lee, M. -S. Jung, N. Kim, J. M. Kim, *J. Phys. Chem. B.*, 2006, **110**, 23812.
39 D. M. Kim, S. P. Park, T. J. Lee, S. G. Hahm, K. Kim, J. C. Kim, W. Kwon, M. Ree, *Langmuir.*, 2009, **25**, 11713.